Supporting Information

19.5% Efficiency Organic Solar Cells Enabled by Direct C-H Arylation-Derived Wide-bandgap Small-molecule Guest Donor

Bin Hu [a], Shenzheng Gao [b], Xin Wang [a], Fan Cao [a], Yiyu Chen [a], Jianqi Zhang [d], Laju Bu [e], Xin Song, *[b,c] and Guanghao Lu *[a]

[a] B. Hu, X. Wang, F. Cao, Y.Chen and G. Lu
Frontier Institute of Science and Technology, and State Key Laboratory of Electrical Insulation and Power Equipment, Xi'an Jiaotong University, Xi'an, Shaanxi 710054, P. R. China. E-mail: guanghao.lu@mail.xjtu.edu.cn

[b] S. Gao, X. Song
School of Materials Science and Engineering, Jiangsu Engineering Laboratory of Light-Electricity-Heat Energy-Converting Materials, Applications, and Jiangsu Collaborative Innovation Center of Photovoltaic Science and Engineering, Changzhou University, Changzhou 213164, P. R. China. E-mail: xin.song@cczu.edu.cn

[c] X. Song
State Key Laboratory of Luminescent Materials and Devices, South China University of Technology, Guangzhou 510640, P. R. China

[d] J. Zhang
CAS Key Laboratory of Nanosystem and Hierarchical Fabrication, CAS Center for Excellence in Nanoscience, National Center for Nanoscience and Technology, Beijing, 100190, P. R. China

[e] L. Bu
School of Chemistry, Xi'an Jiaotong University, Xi'an, 710049, P. R. China

Table of Contents

1. Materials and Methods

Materials: All reagents and solvents, unless otherwise specified, were purchased from commercial sources and were used without further purification. Solvents were dried and purified using standard techniques. All reactions were carried out under argon atmosphere and used standard Schlenk techniques. The detialed synthesis route of *o*PhFO are shown in Scheme S1. 1,4-dibromo-2-fluoro-3-methoxybenzene and TTTP-7-CHO were synthesized according to the previous reports.[1-3] PM6, BTP-ec9 was purchased from Solarmer Materials Inc. PEDOT:PSS and 2PACz was purchased from Xi'an Yuri Solar Co., Ltd. PNDI-F3N-Br was purchased from Nanjing Zhiyan Technology Co., Ltd.

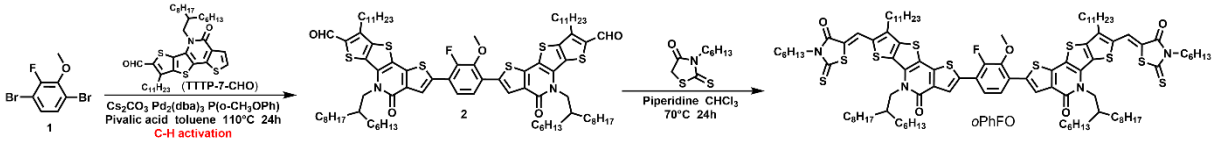

Scheme S1. Synthetic routes for *o*PhFO.

Synthesis of compound 1

1,4-dibromo-2,3-difluorobenzene (2 g, 7.36 mmol), sodium methoxide (0.437 g, 8.09 mmol) and anhydrous tetrahydrofuran (40 mL) was added to 250 mL Schlenk reaction tube under Ar atmosphere. The reaction mixture was stirred at 90 ℃ for 24 h. Then, the reaction mixture was cooled to room temperature and extracted with dichloromethane three times. The combined organic phase was washed with water for three times and dried over anhydrous sodium sulfate. After solvent was evaporated under reduced pressure the residue was purified through a silica gel column with hexane/dichloromethane (100:1, v/v) as eluent to give compound 1 as a white solid (1.7 g, 81.4 %).^{1}H NMR (400 MHz, $CDCl_3$, ppm) δ: 7.22 (dd, J = 8.7, 1.7 Hz, 1H), 7.15 (dd, J = 8.7, 6.3 Hz, 1H), 3.97 (s, 3H). ^{13}C NMR (100MHz, $CDCl_3$, ppm) δ: 153.31, 146.44, 128.63, 128.08, 116.67, 109.43, 61.75. ^{19}F NMR (376 MHz, $CDCl_3$, ppm) δ: -119.62.

Synthesis of compound 2

1,4-dibromo-2-fluoro-3-methoxybenzene (110 mg, 0.3874 mmol), TTTP-7-CHO (597 mg, 0.89 mmol), $Pd_2(dba)_3$ (17.74 mg, 0.0194 mmol), $P(o\text{-}CH_3OPh)_3$ (13.65 mg, 0.0387 mmol), Cs_2CO_3 (379 mg, 1.16 mmol), trimethylacetic acid (15.8 mg, 0.155 mmol) and anhydrous toluene (6 mL) was added to 100 mL Schlenk reaction tube under Ar atmosphere. The reaction mixture was stirred at 110 ℃ for 24 h. Then, the reaction mixture was cooled to room temperature and extracted with dichloromethane three times. The combined organic phase was washed with water for three times and dried over anhydrous sodium sulfate. After solvent was

evaporated under reduced pressure the residue was purified through a silica gel column with hexane/dichloromethane (1:1.5, v/v) as eluent to give compound 2 as a orange-red solid (445 mg, 78.52%). ^{1}H NMR (400 MHz, $CDCl_3$, ppm) δ: 9.98 (s, 1H), 9.97 (s, 1H), 7.95 (s, 1H), 7.93 (s, 1H), 7.40 (d, *J* = 8.7 Hz), 7.18 (t, *J* = 7.7 Hz, 1H), 4.30 (br, 4H), 4.11 (s, 3H), 3.05-3.01 (m, 4H), 2.13-2.07 (m, 2H), 1.84-1.77 (m, 4H), 1.44-1.21 (m, 80H), 0.90-0.83 (m,18H). ^{13}C NMR (100MHz, $CDCl_3$, ppm) δ: 181.45, 158.07, 157.93, 153.59, 151.08, 144.23, 144.02, 141.59, 140.49, 139.23, 139.10, 139.02, 138.98, 136.35, 135.25, 134.10, 133.84, 132.24, 129.89, 128.88, 126.12, 125.10, 123.68, 121.56, 121.03, 120.94, 118.37, 118.00, 61.25, 61.18, 50.27, 37.73, 32.00, 31.96, 31.89, 31.03, 30.25, 30.23, 30.14, 29.82, 29.74, 29.72, 29.66, 29.63, 29.48, 29.43, 29.38, 27.96, 26.38, 26.36, 22.77, 22.74, 22.72, 14.20, 14.18, 14.17. ^{19}F NMR (376 MHz, $CDCl_3$, ppm) δ: -128.79.

Synthesis of *o*PhFO

Compound 2 (200 mg, 0.1367 mmol), 3-hexyl-2-thioxo-1,3-thiazolidin-4-one (297 mg, 1.367 mmol), anhydrous chloroform (15 mL) and pyridine (0.03 mL) was added to 100 mL Schlenk reaction tube under Ar atmosphere. The reaction mixture was stirred at 70 ℃ for 24 h. Then, the reaction mixture was extracted with dichloromethane three times and dried over anhydrous sodium sulfate. After solvent was evaporated under reduced pressure, the residue was purified through a silica gel column with hexane/dichloromethane (1:1, v/v) as eluent to give Compound *o*PhFO as a dark red solid (210 mg, 82 %). ^{1}H NMR (400 MHz, $CDCl_3$, ppm) δ: 7.79 (s, 1H), 7.74 (s, 1H), 7.68 (s, 1H), 7.64 (s, 1H), 7.18 (br, 1H), 6.94 (s, 1H), 4.23(br, 4H), 4.04 (s, 3H), 3.91 (t, *J* = 6.3 Hz, 4H), 2.88 (t, *J* = 6.2 Hz, 4H), 2.03-1.99 (m, 2H), 1.80-1.74 (m, 4H), 1.62-1.25 (m, 96H), 0.91-0.84 (m, 24H). ^{13}C NMR (100MHz, $CDCl_3$, ppm) δ: 190.21, 166.90, 166.81, 157.90, 157.79, 152.73, 150.22, 143.43, 143.31, 141.13, 141.03, 140.08, 140.01, 139.79, 135.49, 134.69, 134.37, 134.23, 134.20, 134.01, 133.73, 130.34, 130.19, 129.05, 128.20, 125.32, 124.40, 123.15, 121.99, 120.99, 120.57, 120.47, 120.37, 120.22, 116.88, 116.57, 60.94, 60.85, 49.98, 44.80, 38.87, 32.13, 32.11, 32.08, 32.06, 31.20, 31.16, 30.98, 30.64, 30.32, 30.15, 30.09, 29.90, 29.85, 29.83, 29.71, 29.62, 29.52, 29.51, 28.65, 26.79, 26.72, 26.48, 22.94, 22.87, 22.83, 22.57, 14.28, 14.26, 14.24, 14.02. ^{19}F NMR (376 MHz, $CDCl_3$, ppm) δ: -128.46. MALDI-TOF MS: calcd for $C_{103}H_{147}FN_4O_5S_{10}$ $[M+H]^+$, 1861.938; found: 1861.832.

2. Measurements and Instruments

Nuclear magnetic resonance (NMR) and Matrix-assisted laser desorption/ionization–Time of Flight (MALDI-TOF). ^{1}H, ^{9}F and ^{13}C NMR spectra were obtained on a Bruker Advance 500 II (400 MHz) NMR spectrometer. ^{1}H, ^{9}F and ^{13}C NMR spectra were referenced

to tetramethylsilane (0 ppm) for $CDCl_3$. The NMR chemical shifts were reported in ppm (parts per million) relative to the residual solvent peak at 7.26 ppm (chloroform) for the ^1H NMR spectroscopy and 77.6 ppm (chloroform) for the ^{13}C NMR spectra.The splitting patterns were designated as follows: s (singlet); d (doublet); t (triplet); m (multiplet). MALDI-TOF mass spectra were measured on the Bruker 4800 MALDI-TOF analyzer.

Optical characterizations. UV-vis absorption spectra were recorded on PerkinElmer Lambda 35 UV-vis spectrophotometer. The solution optical absorption spectra of *o*PhFO were recorded from the concentration of 10^{-6} M in chloroform at room temperature. The thin films sample were spin-coated (10 mg/mL in chloroform solutions, 3000 rpm) onto quartz plates at room temperature. The photoluminescence (PL) spectra were tested by using steady state & lifetime fluorescence spectrometer FLS1000 equipment.

Thermogravimetric analysis (TGA) and differential scanning calorimetry (DSC). TGA was carried out on a METTLER TOLEDO TGA/DSC3$^+$ analyzer under protection of nitrogen at a heating rate of 10 ℃ min^{-1}, and using Al_2O_3 crucibles. Crystallization properties were investigated from heating/cooling cycles from 25 to 300 ℃ at a rate of 10 ℃ min^{-1} with TA Instruments DSC 250.

Electrochemical characterizations. Cyclic voltammetry (CV) were done on a CHI660D electrochemical workstation with glassy carbon, Ag/Ag^+ electrode and a platinum wire as working electrode, reference electrode and counter electrode, respectively, in a tetrabutylammoniumhexafluorophosphate ($[Bu_4N]^+[PF_6]^-$, 0.1 M) acetonitrile solution under the argon atmosphere. The chloroform solution (5 mg/mL) for *o*PhFO were dropped on the surface of glassy carbon electrode to form their corresponding film, respectively. A ferrocene-ferrocenium (F_c/F_c^+) redox couple was used as an internal standard and was assigned an absolute energy of −4.8 eV *vs* vacuum. The HOMO and LUMO energy levels of *o*PhFO were determined according to the equation $E_{HOMO/LUMO} = -(E_{onset,\ ox/red} - E_{Fc/Fc+} + 4.80)$[4].

Contact Angle Measurements and Interfacial Tension Calculation: The contact angles were measured by a contact angle meter (KRUSS DSA100S). The droplets of water and ethylene glycol (EG) were dripped on the *o*PhFO, PM6 and BTP-ec9 neat films. The surface tension (γ) is estimated by the Wu method[5], in which:

$$\gamma_{Water}(\cos\theta_{Water} + 1) = \frac{4\gamma^{d}_{water} \times \gamma^{d}}{\gamma^{d}_{water} + \gamma^{d}} + \frac{4\gamma^{p}_{water} \times \gamma^{p}}{\gamma^{p}_{water} + \gamma^{p}} \quad (1\text{-}1)$$

$$\gamma_{EG}(\cos\theta_{EG} + 1) = \frac{4\gamma^{d}_{EG} \times \gamma^{d}}{\gamma^{d}_{EG} + \gamma^{d}} + \frac{4\gamma^{p}_{EG} \times \gamma^{p}}{\gamma^{p}_{EG} + \gamma^{p}} \quad (1\text{-}2)$$

$$\gamma = \gamma^{d} + \gamma^{p} \quad (1\text{-}3)$$

where θ is the contact angle of each thin film, and γ is the surface tension of samples, which is equal to the sum of the dispersion (γ^{d}) and polarity (γ^{p}) components; γ_{Water} and γ_{EG} were the surface tensions of the water and ethylene glycol; and γ^{d}_{water}, γ^{p}_{water}, γ^{d}_{EG} and γ^{p}_{EG} were the dispersion and polarity components of γ_{Water} and γ_{EG}.

The Flory-Huggins parameter[6] χ_{AB} can be estimated from the surface energy following equation:

$$\chi_{AB} = (\sqrt{\gamma_A} - \sqrt{\gamma_B})^2 \quad (1\text{-}4)$$

The interfacial surface energy can be calculated by Neumann's equation[7] as follow:

$$\gamma_{A:B} = \gamma_A + \gamma_B - 2e^{[-\beta(\gamma_A - \gamma_B)]}\sqrt{\gamma_A\gamma_B} \quad \beta = 0.000115\ m^4\ mJ^{-2} \quad (1\text{-}5)$$

The location of *o*PhFO in the ternary blends was predicted by calculating the wetting coefficient (ω) following the Young's equation and Neumann's equation[8]:

$$\omega_C = (\gamma_{C:B} - \gamma_{C:A})/\gamma_{A:B} \quad (1\text{-}6)$$

where $\gamma_{A:B}$ represents the interfacial tension between two components of A and B (If the wetting coefficient is larger than unity, namely, $\omega_C > 1$, the third component C should be located in the domain A. If $\omega_C < -1$, C should be distributed in the domain B. If $-1 < \omega_C < 1$, C should be located at the interface between A and B).

Devices fabrication. The photovoltaic devices were fabricated with conventional structures of ITO/2PACz/active layers/ PNDI-F3N-Br/Ag. The patterned ITO glass substrates were cleaned sequentially under sonication with deionized water, acetone and isopropanol, and then dried at 60 ℃ in a baking over overnight. After UV-ozone treatment for 20 min, ITO substrates were then dipped into 2PACz solution (0.35 mg/mL, ethanol) with a temperature of 80 ℃ for 10 min, then taken out and washed by pure ethanol. Sequentially, PM6:BTP-ec9 and PM6:*o*PhFO:BTP-ec9 blends (1:1, 1:0.1:1, 1:0.15:1 and 1:0.25:1) were dissolved in chlorobenzene under 100 °C for 4 h to mix intensively in a N_2-filled glove box, in which the PM6:BTP-ec9 solid concentration is 20 mg/mL in total. After that, PNDI-F3N-Br solution with a concentration of 1.0 mg/mL (methanol) was spin-coated on the active layer at 3000 rpm for 30 s. To complete the fabrication of the devices, 100 nm of Ag was thermally evaporated through a mask under a vacuum of ~2×10^{-4} pa. The active area of the devices was 0.04 cm^2.

***J*-*V* and EQE measurement.** The photovoltaic performance was characteristed under an AM 1.5G spectrum from a solar simulator (Newport). The light intensity of light source was calibrated before the testing by using a standard silicon solar cell, as calibrated by a National Renewable Energy Laboratory (NREL) certified silicon photodiode, giving a value of 100 mW/cm^2 in the test. The current density-voltage (*J*-*V*) curves were recorded with a Keithley 2400 source meter. The external quantum efficiency (EQE) spectra were obtained on a commercial EQE measurement system (Taiwan, Enlitech, QE-R3011) in air atmosphere. The light intensity at each wavelength was calibrated by a standard single-crystal Si photovoltaic cell.

Transient photocurrent/photovoltage (TPC/TPV) measurements. In the TPC and TPV measurements, the OSCs were fabricated with the same method as mentioned above. The data were obtained by the all-in-one characterization platform, Paios (Fluxim AG, Switzerland).

Space charge limited current (SCLC) measurements. The mobilities were measured by using a space charge limited current (SCLC) model, Hole-only or Electron-only devices were fabricated as follows: the hole-only device of ITO/PEDOT:PSS/active layer/MoO_3/Ag and electron-only device of ITO/ZnO/active layer/PNDI-F3N-Br/Ag. Hole mobility and electron mobility were obtained by fitting the current density-voltage curves and calculated by the Mott-Gurney equation[9]:

$$J = 9\varepsilon_0\varepsilon_r\mu(V_{app} - V_{bi} - V_s)^2/8L^3$$

where J is current density, ε_0 is the permittivity of free space, ε_r is the relative dielectric constant of the material (assumed to 3), μ is hole mobility or electron mobility, V_{appl} is the applied voltage for device, V_{bi} is the buit-in voltage due to the relative work function difference of the two elcetrodes, V_s is the voltage drop from the substrate's series resistance (V_s = IR), L is the thickness of active layer. The mobility was calculated from the slope of the $J_{1/2}$-V curves. The thickness of the BHJ blend for SCLC measurement was about 100 nm.

Atomic force microscope (AFM) and transmission electron microscopy (TEM). The AFM images were obtained by using a Bruker INNOVA atomic force microscope in tapping mode. The sample for AFM measurements were prepared using the same preparation process those for fabricating devices. The TEM measurements was performed using JEOL JEM-2100 at 200 kV. The samples for TEM measurements were prepared by spin casting the blend solution on

ITO/PEDOT:PSS substrate, then floating the films on a water surface, and transferring to TEM grids.

Grazing incidence wide-angle X-ray scattering (GIWAXS) characterization. GIWAXS measurements were performed on a XEUSS SAXS/WAXS system. The wavelength of the X-ray beam is 1.5418 Å, and the incident angle was 0.2°. Scattered X-rays were detected by using a Dectris Pilatus 300 K photon counting 2D detector.

In-situ UV-vis absorption and photoluminescence spectroscopy. According to the preparation process of the devices, the active layer solution was spin-coated on clean quartz flakes. In this process, the in-situ UV-vis absorption spectra, photoluminescence spectra and light scattering spectra were obtained on a multi-spectrometer (DU-200, Shaanxi Puguang Weishi Co. Ltd.).

Film-depth-dependent light absorption spectroscopy (FLAS). The FLAS spectra was obtained upon a film-depth dependent light absorption spectrometer (PU100, Puguangweishi Co. Ltd). In-situ oxygen plasma etching at low perssure (< 25 Pa) was used to extract the depth-dependent absorption spectrum for the organic active layer. The film-depth-dependent exciton generation is obtained upon the modified optical transfer matrix method, taking film-depth-dependent light absorption spectra and optical interference into simulation. The detail of FLAS characterization is available in the literature[10-13].

Femtosecond transient absorption (TA). The TA measurements of PM6:BTP-ec9 and PM6:*o*PhFO:BTP-ec9 were carried out by the following equipment setup. In this system, a femtosecond laser (PHAROS, light conversion) operating at a 100 kHz repetition rate was selected as the light source of the Femto-TA100 spectrometer (Time-Tech Spectra, Co., Ltd). The pulse duration is around 233 fs, and the output wavelength is 1,030 nm. Then, the fundamental laser beam was split into two. One was introduced into an optical parametric amplifier (OPA, light conversion) to produce a specific wavelength laser as the pump light of Femto-TA100 system. The other was focused onto a sapphire plate or YaG to generate super-continuum white light that served as the probe light. A motorized delay stage was utilized to regulate the time delay between pump and probe light. All measurements were conducted at room temperature under atmospheric conditions.The kinetic process of the blend films at the selected wavelength can be well fitted by triexponential functions ($y = A_1*\exp(-x/\tau_1) + A_2*\exp(-$

$x/\tau_2) + A_3*\exp(-x/\tau_3) + y_0)$, where τ_1 represents the ultrafast exciton dissociation at the at the donor/acceptor interface, τ_2 is releted to the exciton diffusion time toward the interfaces before dissociation, the τ_3 reflects the dynamics of free charges (the value in the time range of hundreds of picoseconds to nanoseconds).[14, 15]

Energy loss. the total E_{loss} value are consist of three parts including ΔE_1 (radiative loss above band gap), ΔE_2 (additional radiative loss below band gap), and ΔE_3 (non-radiative loss). Specification of the three parts of E_{loss} follows the equation:

$$E_{loss} = (E_g - qV_{OC}^{SQ}) + qV_{OC}^{rad,\ below\ gap} + qV_{OC}^{non\text{-}rad} = \Delta E_1 + \Delta E_2 + \Delta E_3$$

where E_g is the band-gap, V_{OC}^{SQ} is the maximum V_{OC} under the Shockley-Queisser limit, and V_{OC}^{rad} is the V_{OC} when only radiative recombination is considered. The final part of the non-radiative recombination loss (ΔE_3) is obtained by the calculation equation:

$$\Delta E_3 = qV_{OC}^{non\text{-}rad} = -kT\ln(EQE_{EL})$$

where k is the Boltzmann constant, T is absolute temperature.

Urbach energy calculation. Since the s-EQE method is suitable for highly sensitive absorption measurements and the EQE is direct proportion to the absorbance according to: The values of E_u could be obtained from the s-EQE curves by an exponential fit.

$$EQE(E) \propto \alpha(E) \propto e^{\frac{E - E_g}{E_u}}$$

$$EQE = Ae^{\frac{E - E_g}{E_u}}$$

$$\ln EQE = \frac{1}{E_u}E + B$$

3. Supplementary Figures and Tables

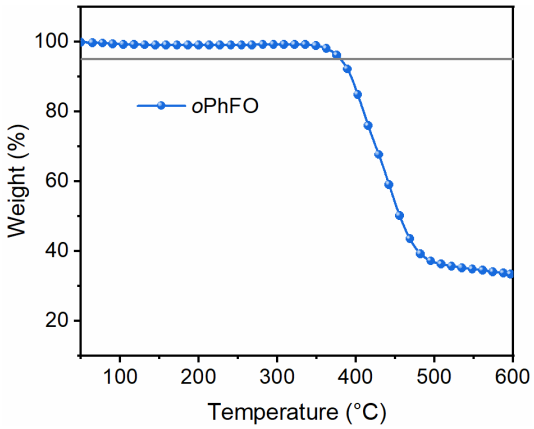

Fig. S1 TGA plots of *o*PhFO.

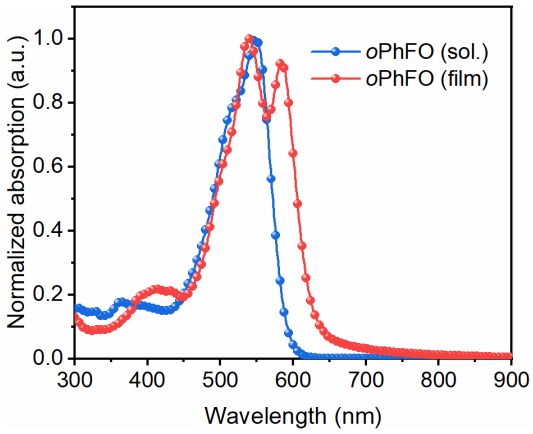

Fig. S2 Normalized UV-vis absorption spectra of *o*PhFO in chloroform solution and neat films, respectively.

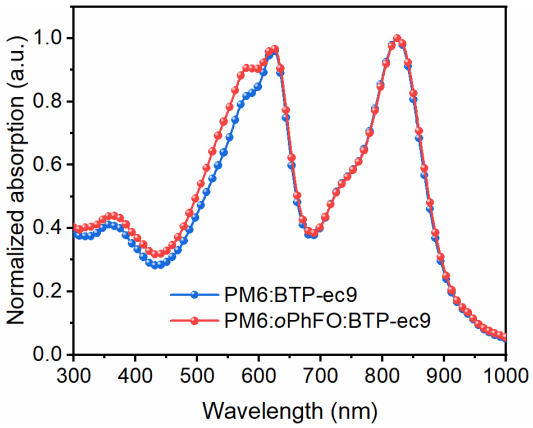

Fig. S3 Absorption spectra of the PM6:BTP-ec9 and PM6:*o*PhFO:BTP-ec9 blend films.

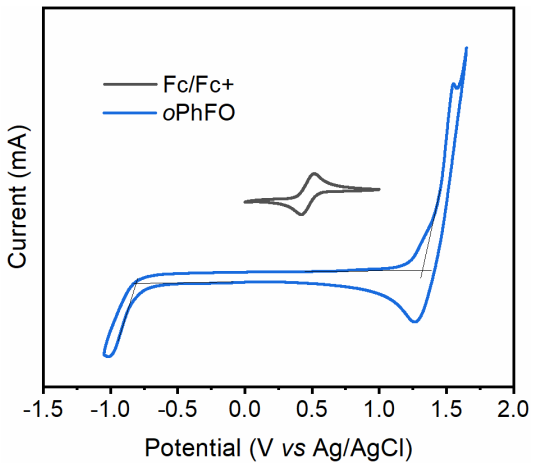

Fig. S4 The cyclic voltammetry (CV) curves of *o*PhFO.

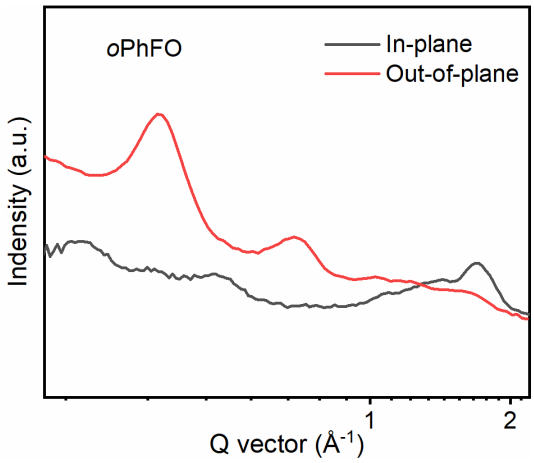

Fig. S5 a) In-plane and Out-of-plane line cut profiles of *o*PhFO neat films.

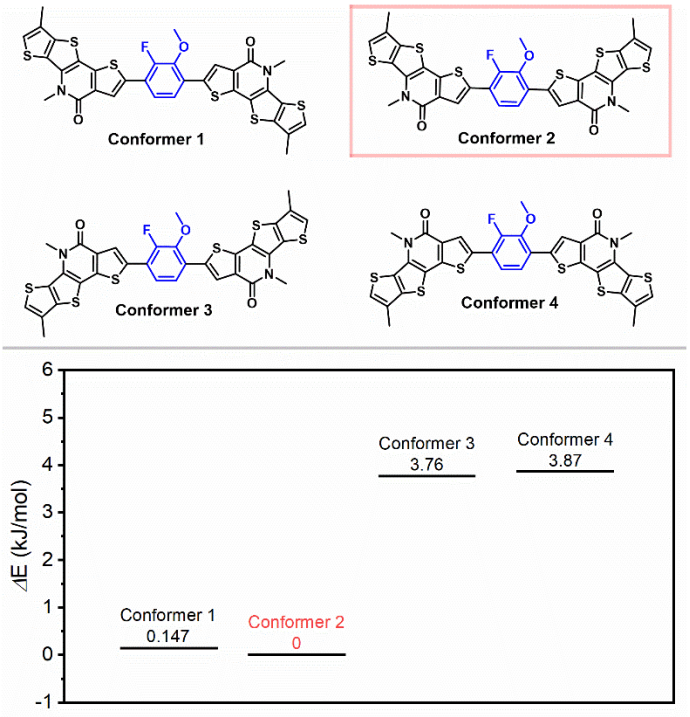

Fig. S6 Four possible conformers of the *o*PhFO and their relative energy.

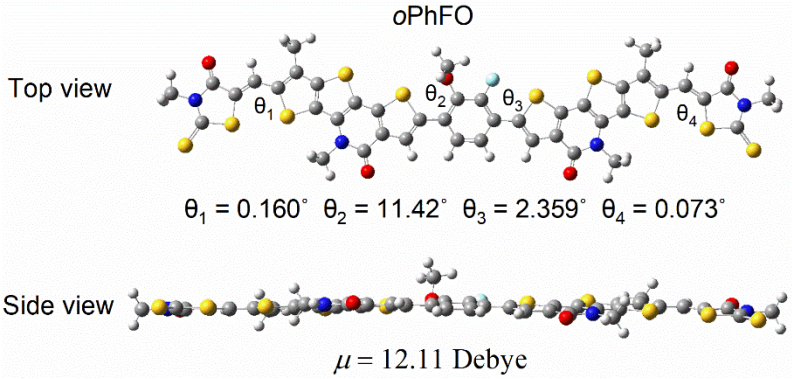

Fig. S7 Optimized molecular geometries of *o*PhFO.

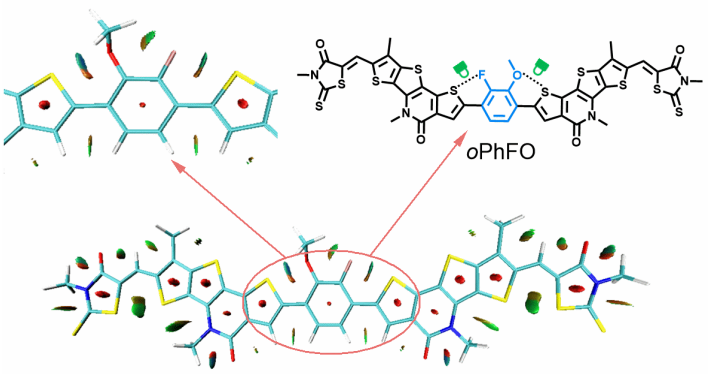

Fig. S8 The RDG isosurface maps of *o*PhFO with an isovalue of 0.5.

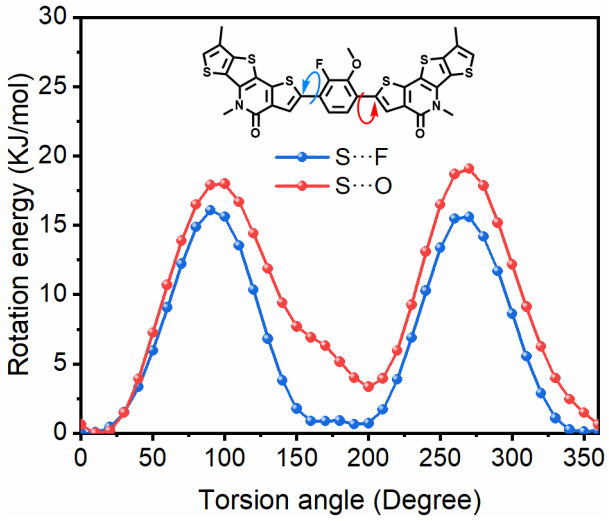

Fig. S9 The relaxed potential energy scan results of *o*PhFO.

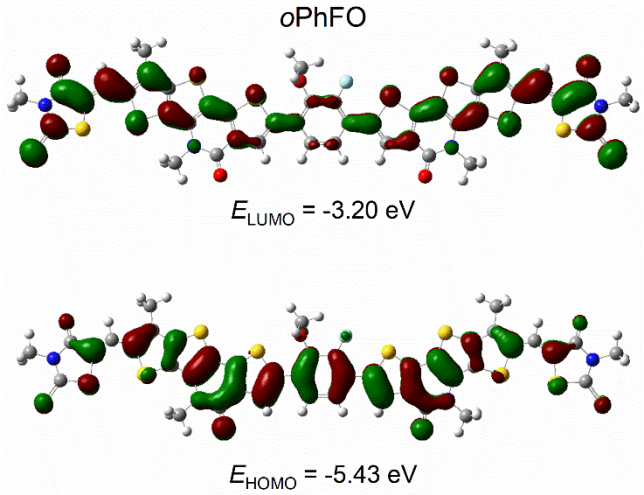

Fig. S10 The density functional theory calculations of HOMO and LUMO energy levels of *o*PhFO, and their iso-density surface of the frontier molecular orbits.

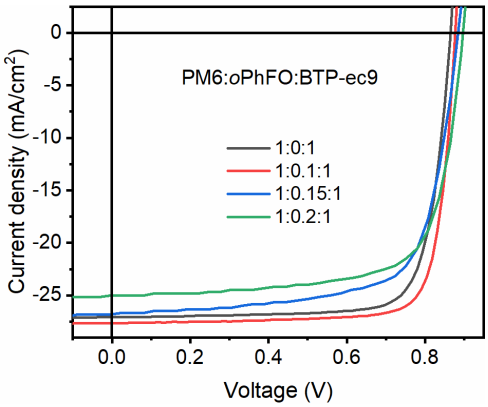

Fig. S11 Photovoltaic parameters of the PM6:*o*PhFO:BTP-ec9 device with different *o*PhFO content.

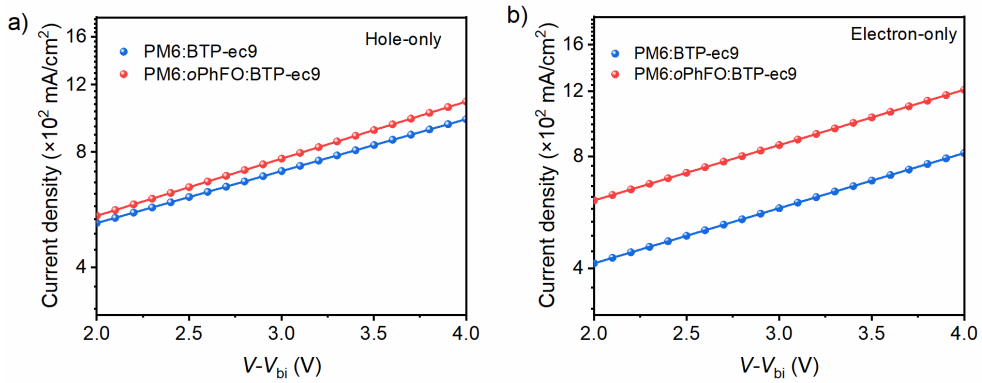

Fig. S12 Dark current density-voltage characteristics at room temperature of PM6:BTP-ec9 and PM6:*o*PhFO:BTP-ec9 blend films for a) hole-only diodes and b) electron-only diodes.

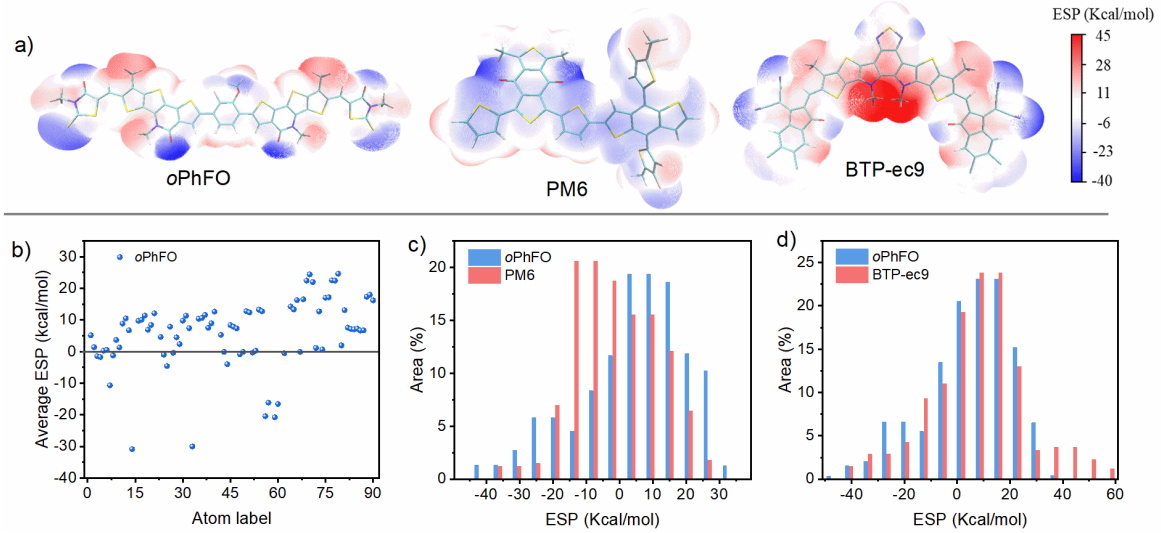

Fig. S13 a) ESP distributions on *o*PhFO, PM6 and BTP-ec9 models. b) ESP statistics of atoms in *o*PhFO models. c) ESP area distributions of *o*PhFO and PM6 models. d) ESP area distributions of *o*PhFO and BTP-ec9 models.

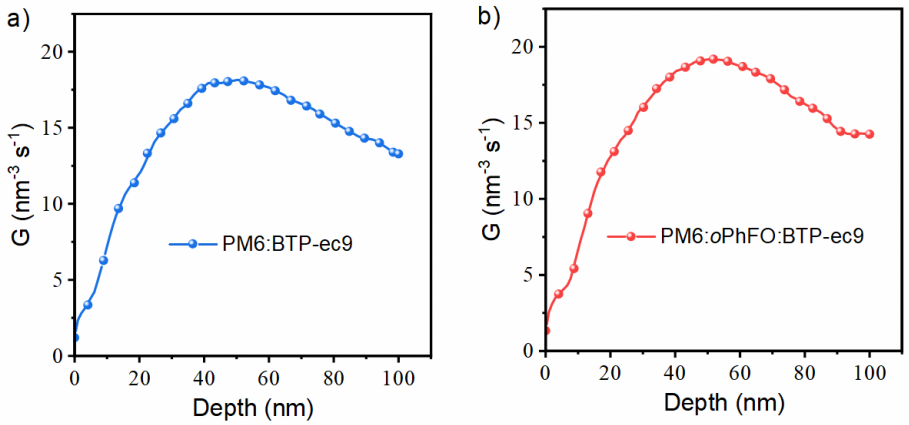

Fig. S14 Simulated exciton generation rate curves as a function of film depth for the optimzed a) PM6:BTP-ec9 and b) PM6:*o*PhFO:BTP-ec9 blend films.

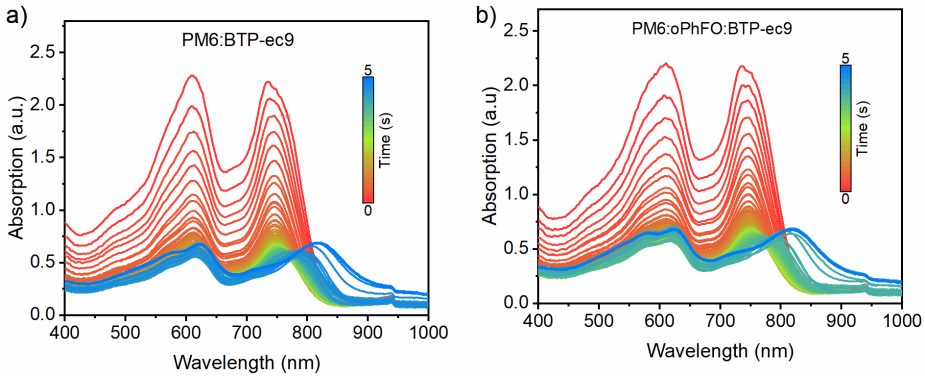

Fig. S15 In-situ UV-vis absorption spectra of the a) PM6:BTP-ec9 and b) PM6:*o*PhFO:BTP-ec9 during the film-drying process.

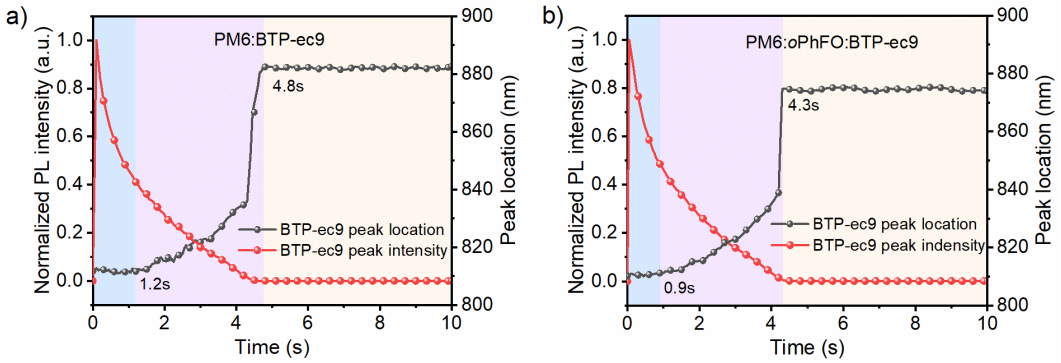

Fig. S16 Time evolution of PL peak location and normalized PL intensity for a) PM6:BTP-ec9, b) PM6:*o*PhFO:BTP-ec9 during the solution evaporated.

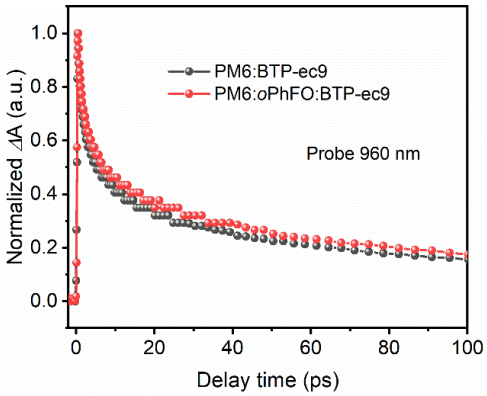

Fig. S17 Kinetic traces probing at around 960 nm for PM6:BTP-ec9 and PM6:*o*PhFO:BTPec9 blends.

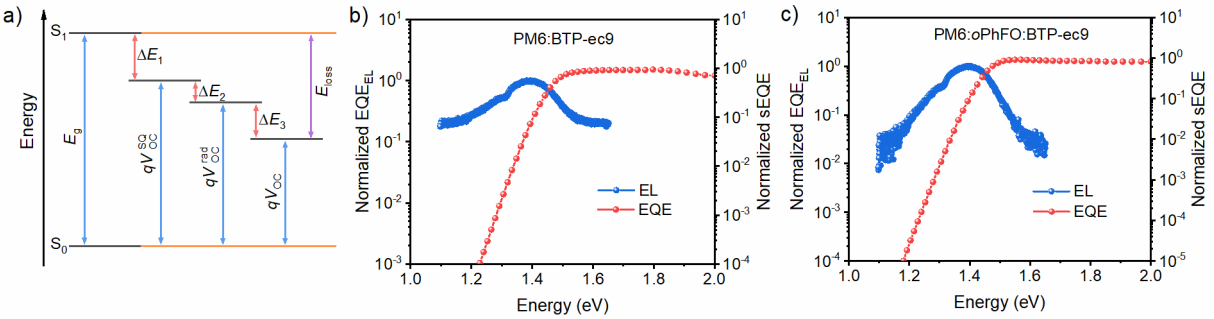

Fig. S18 a) Energy loss diagram of different parts in OSCs. Normalized EQE and EL spectra of a) PM6:BTP-ec9 and b)PM6:*o*PhFO:BTPec9.

Table S1. Optical and electrical properties of *o*PhFO.

Donors	$\lambda_{abs.}^{sol.}$ [a] (nm)	$\lambda_{abs.}^{film}$ [b] (nm)	λ_{onset}^{film} (nm)	$E_g^{opt.}$ [c] (eV)	HOMO [d] (eV)	LUMO [d] (eV)
*o*PhFO	549	539 585	626	1.98	-5.66	-3.54

[a] In dilute chloroform solution (10^{-6} M)

[b] From pristine films spin-coated from chloroform solutions

[c] Calculated from $E_g^{opt.} = 1240/\lambda_{onset}^{film}$

[d] $E_{HOMO/LUMO} = -(E_{onset,\ ox/red} - E_{Fc/Fc+} + 4.80)$

Table S2 Photovoltaic parameters of the PM6:*o*PhFO:BTP-ec9 device with different *o*PhFO content.

PM6:*o*PhFO:BTP-ec9 (D1:D2:A)	V_{OC} (V)	J_{SC} (mA/cm^2)	FF (%)	PCE (%)
1:0:1	0.864	26.9	78.4	18.2
1:0.1:1	0.878	27.6	80.6	19.5
1:0.15:1	0.884	26.8	70.8	16.7
1:0.25:1	0.899	25.1	71.7	16.4

Table S3 Photovoltaic parameters of PM6:*o*PhFO:BTP-ec9 device with different spinning speed

Speed (rpm)	V_{OC} (V)	J_{SC} (mA/cm^2)	FF (%)	PCE (%)
2000	0.870	27.9	78.9	19.2
2500	0.878	27.6	80.6	19.5
3000	0.876	27.1	80.1	19.0
3500	0.878	26.8	80.2	18.9

Table S4 Photovoltaic parameters of PM6:*o*PhFO:BTP-ec9 device with thermal annealing temperature

Temperature (℃)	V_{OC} (V)	J_{SC} (mA/cm^2)	FF (%)	PCE (%)
80	0.878	27.1	78.7	18.7
100	0.878	27.6	80.6	19.5
120	0.865	26.8	78.4	18.1

Table S5 Photovoltaic parameters of the reported D1:D2:A-type ternary OSCs with PCE over 17 % and this work.

	Active layers	V_{OC} (V)	J_{SC} (mA/cm^2)	FF (%)	PCE (%)	Refs.
1	PM6:Y6:DB-1	0.832	27.86	77.9	18.07	[16]
2	PM6:Y6:DB-2	0.836	28.00	77.4	18.20	[16]
3	PM6:Y6:*o*Ph2F	0.860	27.34	75.34	17.72	[3]
4	PM6:Y6:*p*Ph2F	0.859	27.73	77.29	18.40	[3]
5	PM6:Y6: BTID-2F	0.848	27.66	76.36	17.98	[17]
6	PM6:BTID-2F:L8-BO	0.889	26.86	77.52	18.52	[17]
7	PM6:Y6: TTBT-R	0.863	27.38	76.46	18.07	[18]
8	PM6:Y6:S3	0.856	25.86	79.17	17.53	[19]
9	PM6:Y6:BTTzR	0.87	26.2	77.7	17.70	[20]
10	PM6:Y6:G19	0.834	27.85	76.85	17.86	[21]
11	PM6:Y6:BTBR-2F	0.859	27.30	74.11	17.38	[22]
12	PM6:Y6:BTC	0.834	28.0	73.35	17.32	[23]
13	PM6:BTC:L8-BO	0.895	26.74	76.23	18.24	[23]
14	PM6:L8-BO:BTID-2F	0.889	26.86	77.52	18.52	[17]
15	PM6:L8-BO:D18	0.896	26.7	81.9	19.6	[24]
16	PM6:BTP-eC9:BPR-SCl	0.856	27.13	77.6	18.02	[25]
17	PM6:BTP-eC9:PM7-Si	0.864	26.35	77.6	17.7	[26]
18	PM6:BTP-eC9:P-Cl	0.853	27.81	80.50	19.10	[27]
19	PM6:BTP-eC9:PM6-Si30	0.870	26.90	78.04	18.27	[28]

20	PM6:L8-BO:BR-C12	0.881	26.66	77.72	18.26	[29]
21	PM6:BTTC:BTP-eC9	0.853	28.32	79.4	19.18	[30]
22	PM6:BTP-eC9:ADA	0.859	27.58	77.34	18.32	[31]
23	PM6:BTP-eC9:PB2F	0.863	26.8	80.4	18.6	[32]
24	PM6:Y6:BR1	0.859	26.49	75.7	17.23	[33]
25	PM6:*o*PhFO:BTP-eC9	0.878	27.6	80.6	19.5	This work

Table S6 The carrier mobility of PM6:BTP-ec9 and PM6:*o*PhFO:BTP-ec9 devices.

Active layer	Carrier mobility ($\times10^{-4}$ cm^2 V^{-1} s^{-1})		μ_h/μ_e
	μ_h	μ_e	
PM6:BTP-ec9	3.57	2.09	1.71
PM6:*o*PhFO:BTP-ec9	3.99	4.21	0.95

Table S7 The detailed parameters about surface energies of PM6, BTP-ec9, *o*PhFO neat films

Film	γ (mN m^{-1})	$\chi_{PM6:X}$ a) (K)	$\chi_{BTP\text{-}ec9:X}$ a) (K)	$\gamma_{PM6:X}$ b) (mN m^{-1})	$\gamma_{X:PM6}$ b) (mN m^{-1})	$\gamma_{X:BTP\text{-}ec9}$ b) (mN m^{-1})	ω_x c)
PM6	23.89	-	1.189	-	-	-	-
BTP-ec9	35.74	1.189	-	1.109	-	-	-
*o*PhFO	25.87	0.039	0.796	-	0.0507	0.726	0.609

a) $\chi_{PM6:X}$ and $\chi_{BTP\text{-}ec9:X}$ represents the Flory-Huggins interaction parameter between compound PM6 or BTP-ec9 and compound X (*o*PhFO) respectively. b) $\gamma_{X:PM6}$ and $\gamma_{X:BTP\text{-}ec9}$ represents the interfacial surface energy between compound PM6 or BTP-ec9 and compound X (*o*PhFO) respectively. b) ω_x represents the wetting coefficient.

Table S8 Detailed GIWAXS parameters of the binary and ternary blend films.

Active layer	(010) diffraction peak OOP				(100) diffraction peak IP			
	Q [$Å^{-1}$]	D [Å]	FWHM [$Å^{-1}$]	CCL [Å]	Q [$Å^{-1}$]	D [Å]	FWHM [$Å^{-1}$]	CCL [Å]
PM6:BTP-ec9	1.694	3.71	0.249	25.23	0.298	21.08	0.0788	79.33
PM6:*o*PhFO:BTP-ec9	1.737	3.62	0.210	29.92	0.304	20.66	0.0698	89.96

Table S9 Fitted parameters for TA kinetics at PM6 GSB of the binary and ternary blends.

Pump@ 800nm	τ_1	τ_2	τ_3
PM6:BTP-ec9	10.87	74.40	681.8
PM6:*o*PhFO: BTP-ec9	11.13	80.46	728.6

4. Spectral charts of NMR and MALDI-TOF

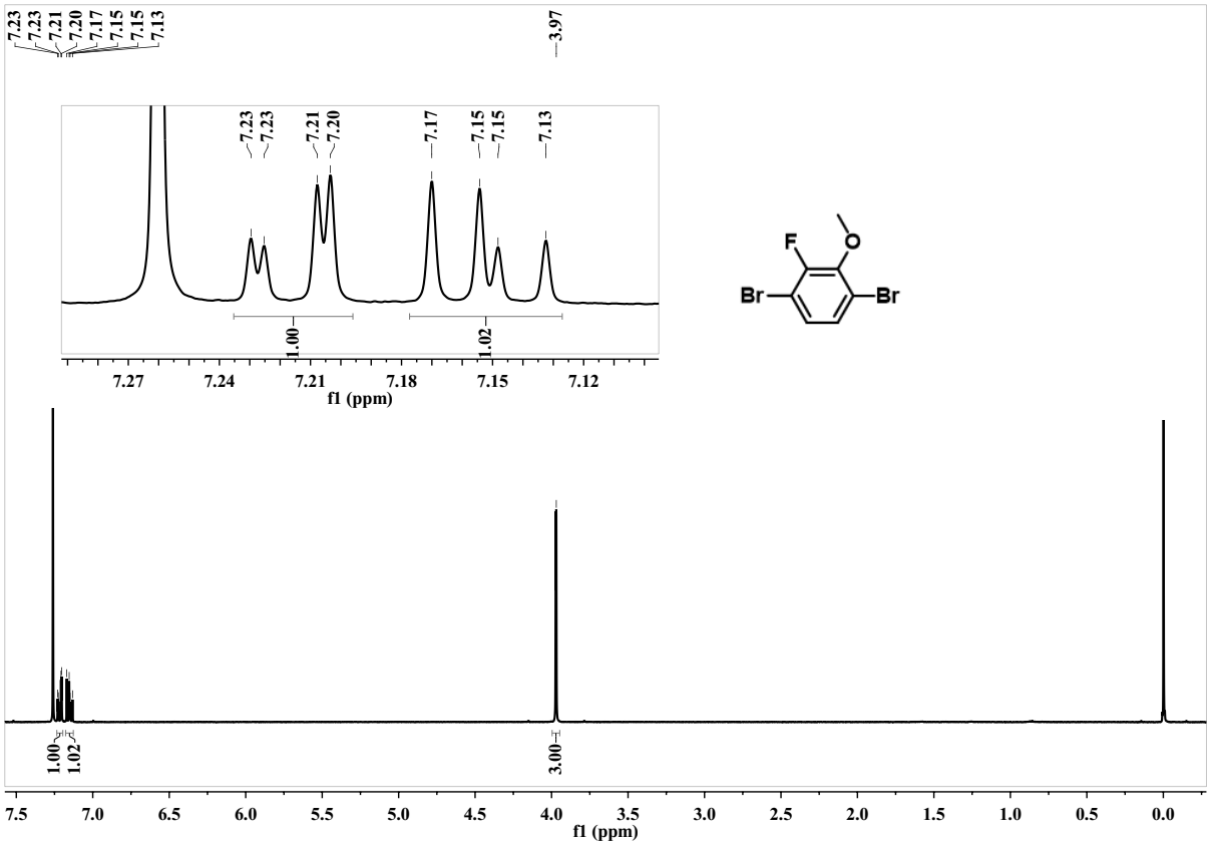

Fig. S19 ^{1}H NMR spectrum of 1 in $CDCl_3$.

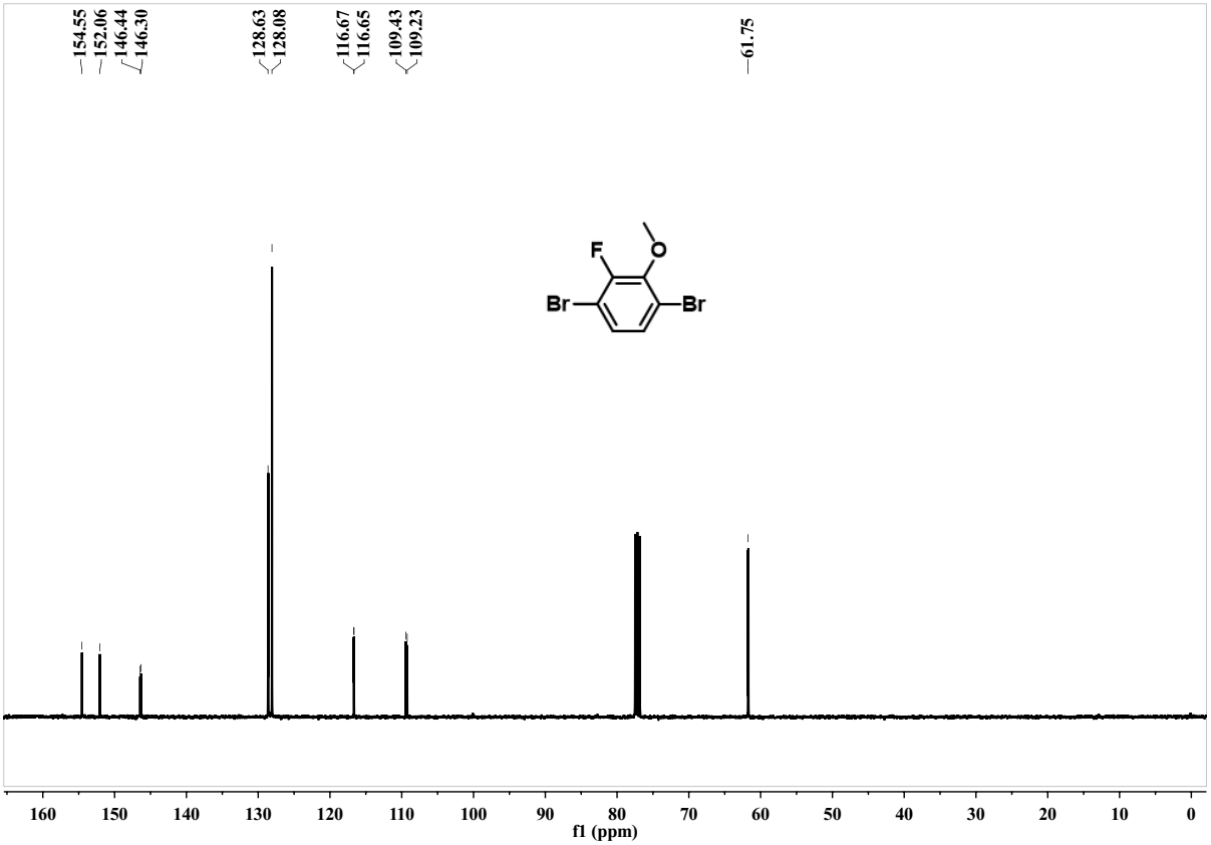

Fig. S20 ^{13}C NMR spectrum of 1 in $CDCl_3$.

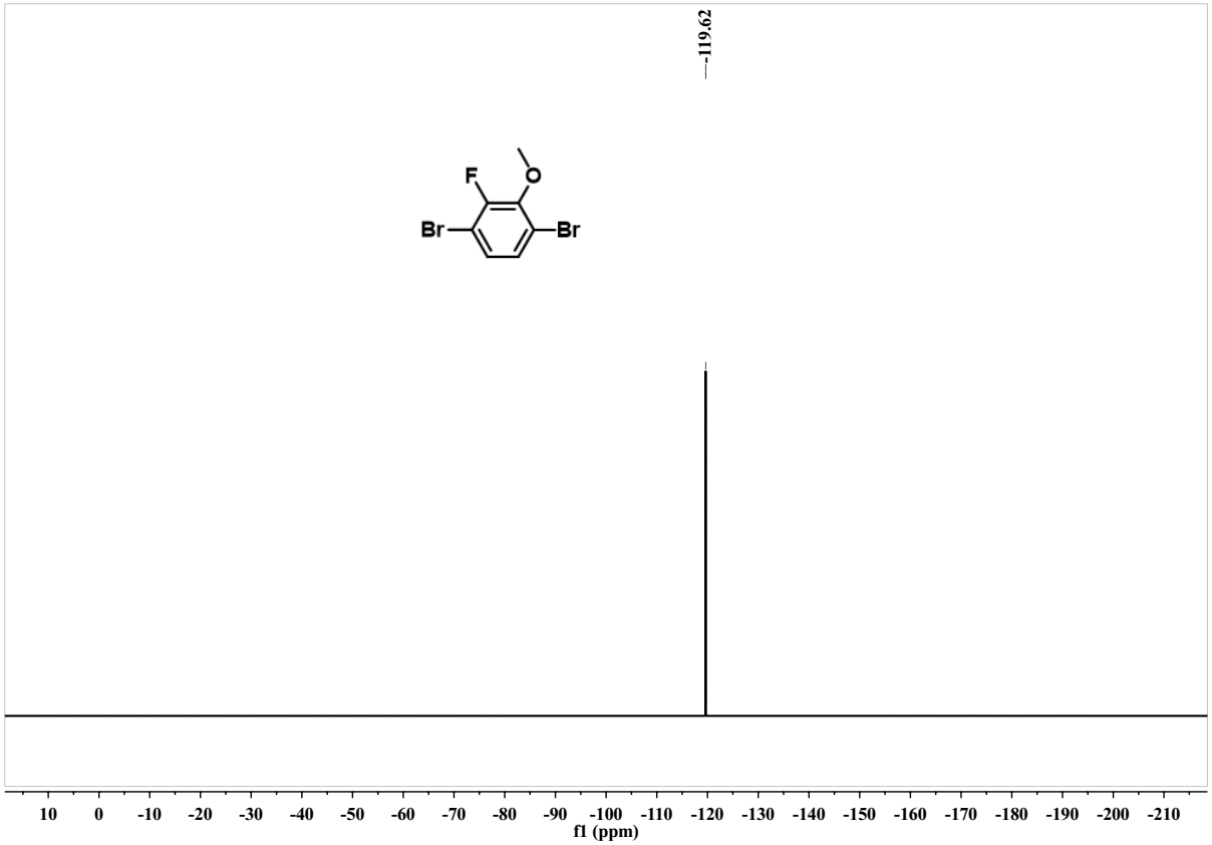

Fig. S21 ^{9}F NMR spectrum of 1 in $CDCl_3$.

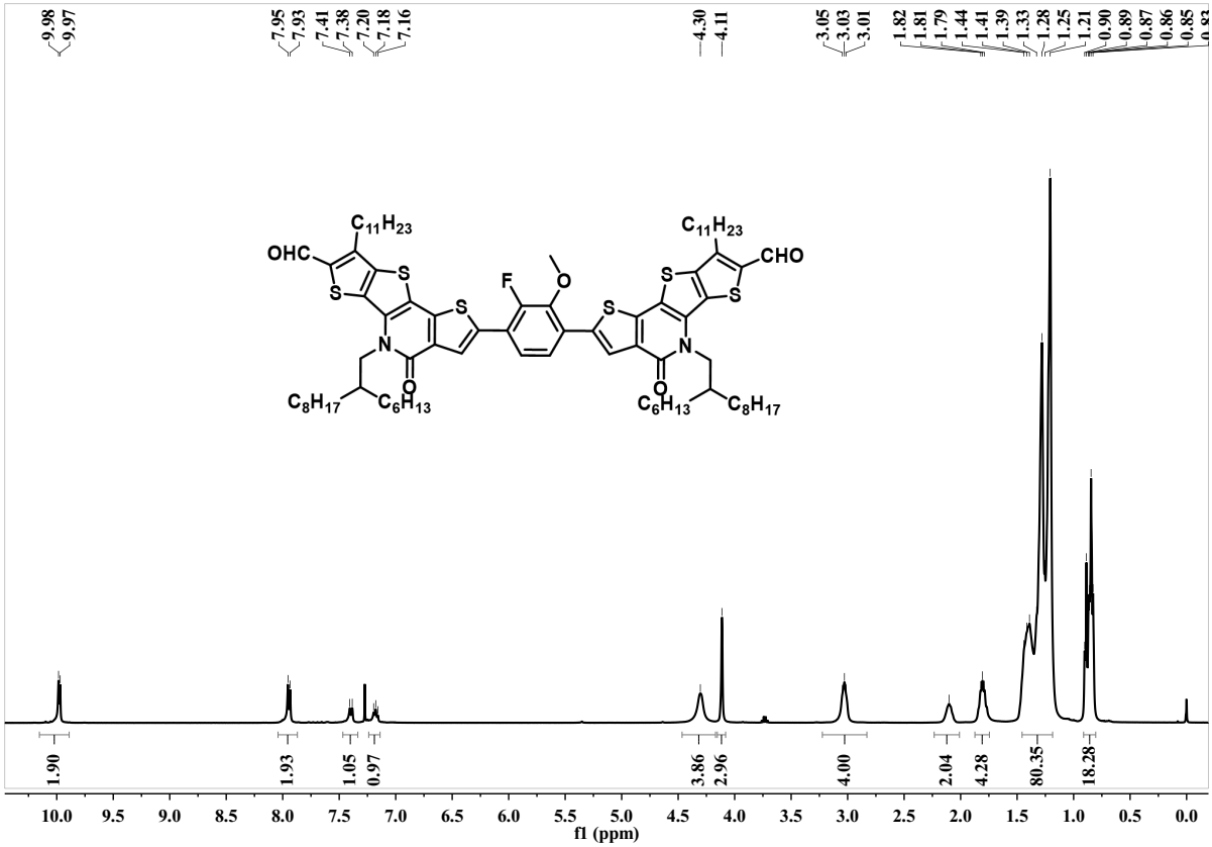

Fig. S22 ^{1}H NMR spectrum of 2 in $CDCl_3$.

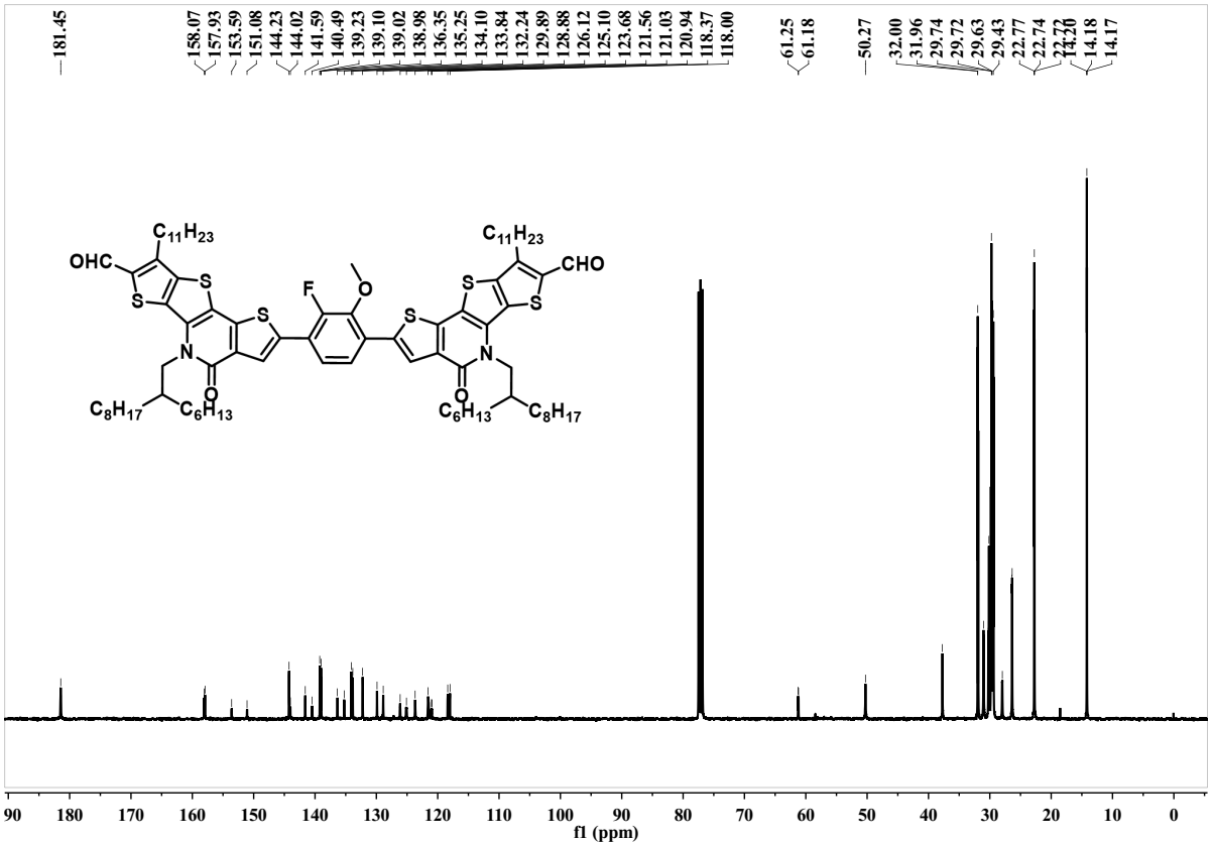

Fig. S23 ^{13}C NMR spectrum of 2 in $CDCl_3$.

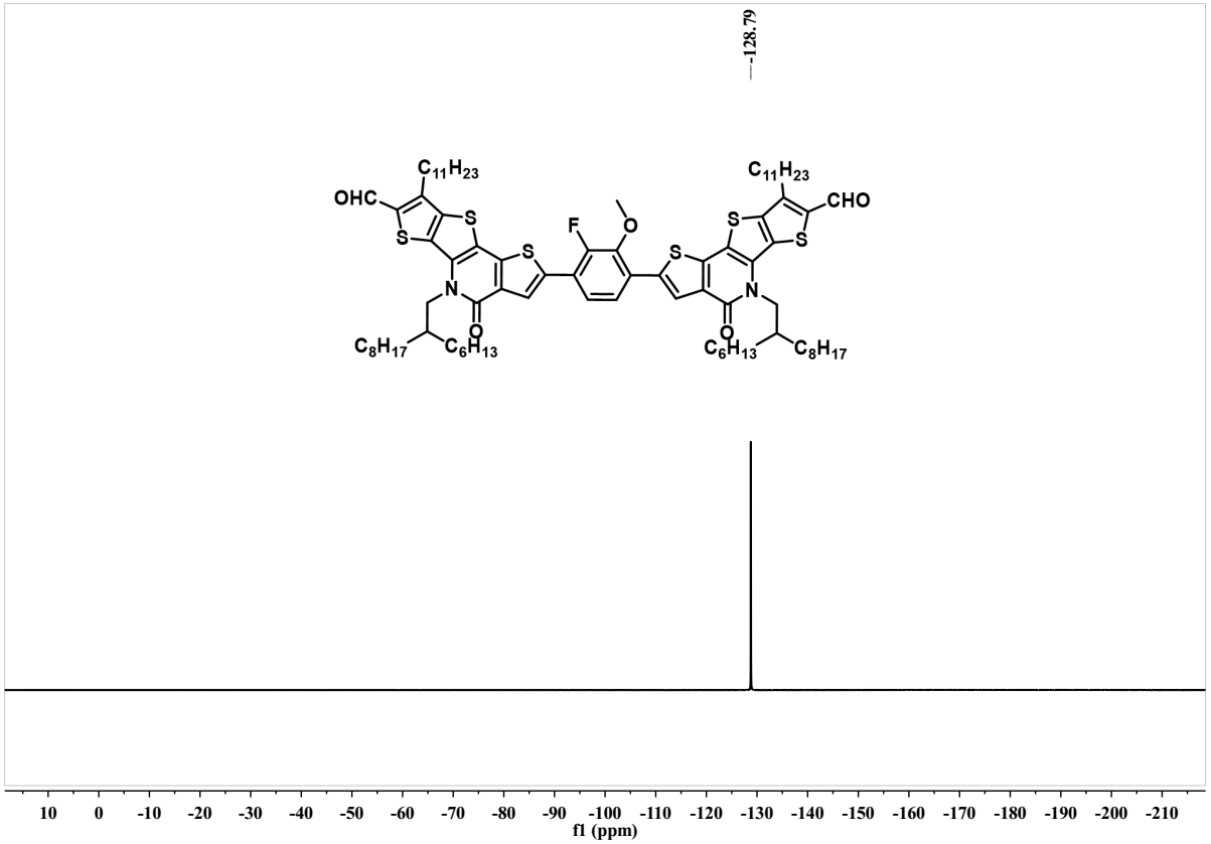

Fig. S24 ^{9}F NMR spectrum of 2 in $CDCl_3$.

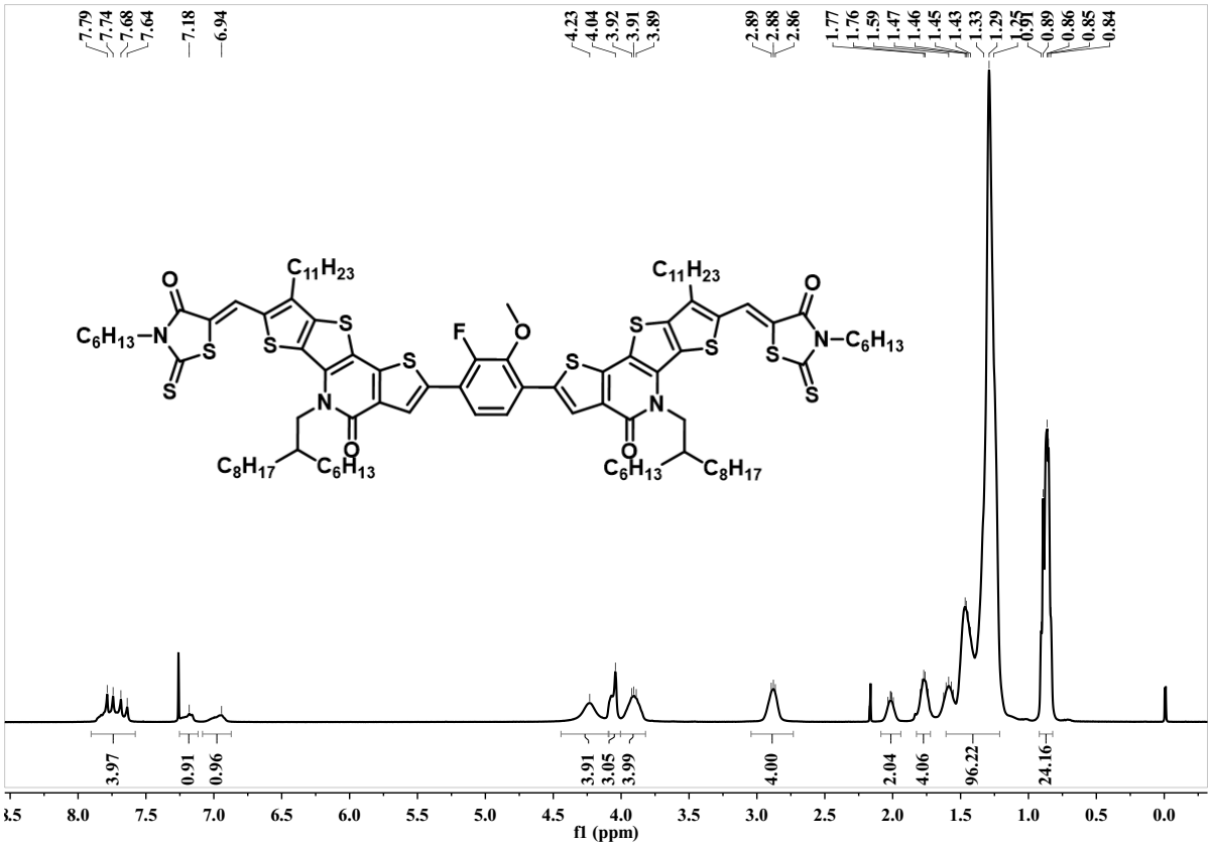

Fig. S25 ^{1}H NMR spectrum of *o*PhFO in $CDCl_3$.

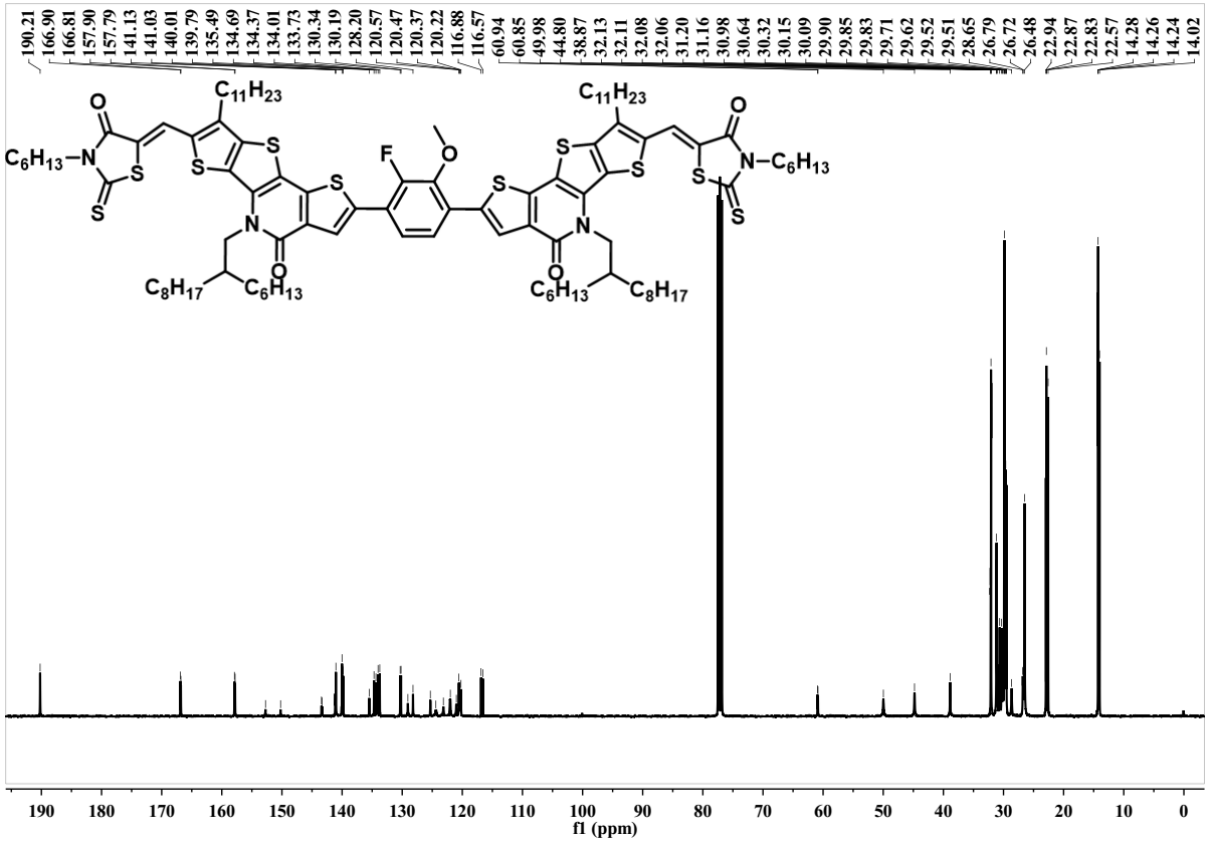

Fig. S26 ^{13}C NMR spectrum of *o*PhFO in $CDCl_3$.

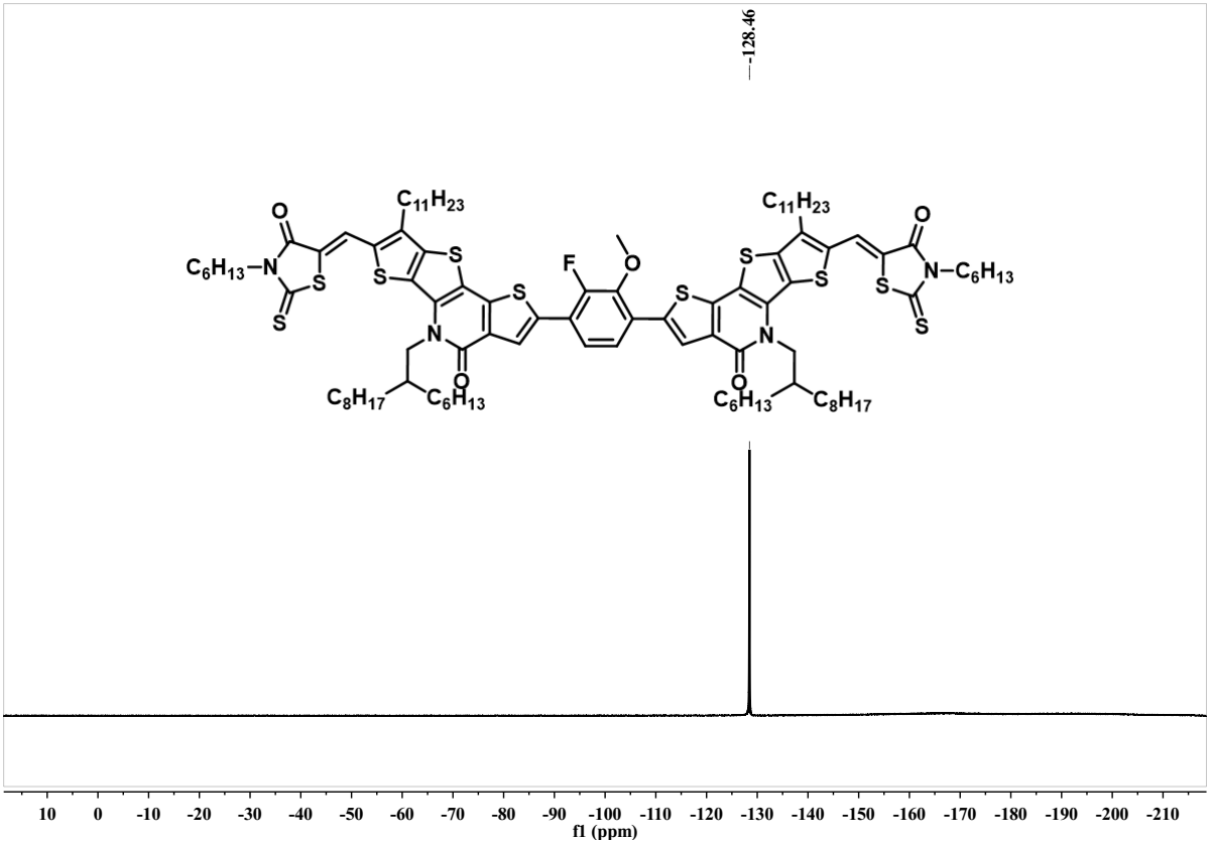

Fig. S27 ^{9}F NMR spectrum of *o*PhFO in $CDCl_3$.

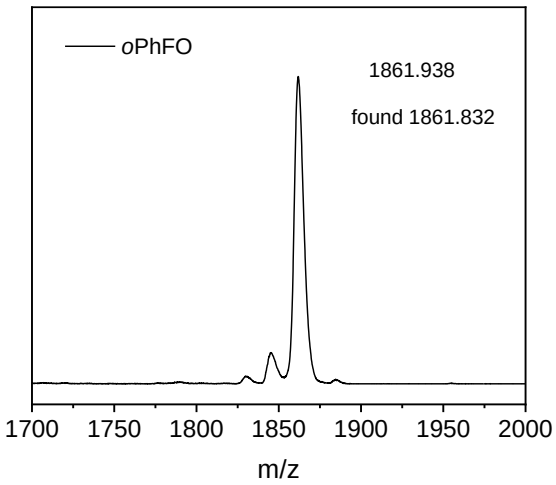

Fig. S28 MALDI-TOF MS spectrum of *o*PhFO.

Refrence

[1] B. Hu, Y. Wang, Z. Shen, X. Wang, M. Zhang, Y. Chen, L. Bu, W. Ma, G. Lu, *Sol Rrl* **2023**, 7, 2300310.

[2] T. Wang, J. Q. Qin, Z. Xiao, J. Q. Zhang, Z. C. Chen, L. X. Zhang, M. Cheng, Z. W. Jin, Y. B. Yuan, W. Q. Wu, C. H. Duan, S. Y. Xie, K. Sun, F. Hao, L. M. Ding, *Nano Energy* **2020**, 77, 105161.

[3] B. Hu, C. Zhang, X. Wang, X. Ding, J. Yu, L. Bu, K. Wang, H. Hu, G. Lu, *Chem. Eng. J.* **2024**, 489, 150968.

[4] D. Li, H. Zhang, X. Cui, Y. N. Chen, N. Wei, G. Ran, H. Lu, S. Chen, W. Zhang, C. Li, Y. Liu, Y. Liu, Z. Bo, *Adv. Mater.* **2023**, 36, 2310362

[5] J. S. Park, N. Choi, C. Lee, S. Lee, J.-W. Ha, D.-H. Hwang, B. J. Kim, *Chem. Mater.* **2020**, 32, 3585.

[6] Z. Cao, J. Chen, S. Liu, M. Qin, T. Jia, J. Zhao, Q. Li, L. Ying, Y.-P. Cai, X. Lu, F. Huang, Y. Cao, *Chem. Mater.* **2019**, 31, 8533.

[7] D. Li, L. Zhu, X. Liu, W. Xiao, J. Yang, R. Ma, L. Ding, F. Liu, C. Duan, M. Fahlman, Q. Bao, *Adv. Mater.* **2020**, 32, 2002344.

[8] Q. An, F. Zhang, Q. Sun, M. Zhang, J. Zhang, W. Tang, X. Yin, Z. Deng, *Nano Energy* **2016**, 26, 180.

[9] S. Chen, Y. Liu, L. Zhang, P. C. Y. Chow, Z. Wang, G. Zhang, W. Ma, H. Yan, *J. Am. Chem. Soc.* **2017**, 139, 6298.

[10] L. Bu, S. Gao, W. Wang, L. Zhou, S. Feng, X. Chen, D. Yu, S. Li, G. Lu, *Adv. Electron. Mater.* **2016**, 2, 1600359.

[11] Z. Wang, Y. Hu, T. Xiao, Y. Zhu, X. Chen, L. Bu, Y. Zhang, Z. Wei, B. B. Xu, G. Lu, *Adv. Opt. Mater.* **2019**, 7, 1900152.

[12] T. Xiao, J. Wang, S. Yang, Y. Zhu, D. Li, Z. Wang, S. Feng, L. Bu, X. Zhan, G. Lu, *J. Mater. Chem. A* **2020**, 8, 401.

[13] F. Z. Cui, Z. H. Chen, J. W. Qiao, T. Wang, G. H. Lu, H. Yin, X. T. Hao, *Adv. Funct. Mater.* **2022**, 32, 2200478.

[14] X. P. Duan, W. Song, J. W. Qiao, X. M. Li, Y. H. Cai, H. B. Wu, J. Zhang, X. T. Hao, Z. Tang, Z. Y. Ge, F. Huang, Y. M. Sun, *Energy Environ. Sci.* **2022**, 15, 1563.

[15] Z. C. Shen, J. D. Yu, G. Y. Lu, K. M. Wu, Q. Y. Wang, L. J. Bu, X. F. Liu, Y. W. Zhu, G. H. Lu, *Energy Environ. Sci.* **2023**, 16, 2945.

[16] H. Wang, D. Yang, P. Ding, L. Xie, Z. Chen, S. Yang, P. Yan, Y. Meng, J. Zhang, Z. Wei, Z. Ge, *Chem. Eng. J.* **2023**, 474, 145395.

[17] Y. Yan, Y. Zhang, Y. Liu, Y. Shi, D. Qiu, D. Deng, J. Zhang, B. Wang, M. A. Adil, K. Amin, W. A. Memon, M. Wang, H. Zhou, X. Zhang, Z. Wei, *Adv. Energy Mater.* **2022**, 12, 2200129.

[18] M. Guan, W. Tao, L. Xu, Y. Qin, J. Zhang, S. Tan, M. Huang, B. Zhao, *J. Mater. Chem. A* **2022**, 10, 9746.

[19] Q. An, J. Wang, X. Ma, J. Gao, Z. Hu, B. Liu, H. Sun, X. Guo, X. Zhang, F. Zhang, *Energy Environ. Sci.* **2020**, 13, 5039.

[20] Q. Liu, Y. Wang, J. Fang, H. Liu, L. Zhu, X. Guo, M. Gao, Z. Tang, L. Ye, F. Liu, M. Zhang, Y. Li, *Nano Energy* **2021**, 85, 105963.

[21] Z. Chen, W. Song, K. Yu, J. Ge, J. Zhang, L. Xie, R. Peng, Z. Ge, *Joule* **2021**, 5, 2395.

[22] L. Xu, W. Tao, H. Liu, J. Ning, M. Huang, B. Zhao, X. Lu, S. Tan, *J. Mater. Chem. A* **2021**, 9, 11734.

[23] C. Zhang, J. Li, L. Ji, H. Hu, G. Li, K. Wang, *J. Mater. Chem. A* **2022**, 10, 22812.

[24] L. Zhu, M. Zhang, J. Xu, C. Li, J. Yan, G. Zhou, W. Zhong, T. Hao, J. Song, X. Xue, Z. Zhou, R. Zeng, H. Zhu, C.-C. Chen, R. C. I. MacKenzie, Y. Zou, J. Nelson, Y. Zhang, Y. Sun, F. Liu, *Nat. Mater.* **2022**, 21, 656.

[25] X. Chen, D. Wang, Z. Wang, Y. Li, H. Zhu, X. Lu, W. Chen, H. Qiu, Q. Zhang, *Chem. Eng. J.* **2021**, 424, 130397.

[26] W. Peng, Y. Lin, S. Y. Jeong, Y. Firdaus, Z. Genene, A. Nikitaras, L. Tsetseris, H. Y. Woo, W. Zhu, T. D. Anthopoulos, E. Wang, *Chem. Mater.* **2021**, 33, 7254.

[27] M. Zhou, C. Liao, Y. Duan, X. Xu, L. Yu, R. Li, Q. Peng, *Adv. Mater.* **2022**, 35, 2208279.

[28] W. Peng, Y. Lin, S. Y. Jeong, Z. Genene, A. Magomedov, H. Y. Woo, C. Chen, W. Wahyudi, Q. Tao, J. Deng, Y. Han, V. Getautis, W. Zhu, T. D. Anthopoulos, E. Wang, *Nano Energy* **2022**, 92, 106681.

[29] Z. Liu, H. Feng, L. Guo, T. Liu, B. Zhao, B. Wu, C. Gao, W. Ma, W. Wu, *Dyes Pigments* **2023**, 217, 111423.

[30] J. Li, C. Zhang, X. Sun, H. Wang, H. Hu, K. Wang, M. Xiao, *Nano Energy* **2024**, 125, 109542.

[31] Y. Cheng, B. Huang, X. Huang, L. Zhang, S. Kim, Q. Xie, C. Liu, T. Heumüller, Z. Liu, Y. Zhang, F. Wu, C. Yang, C. J. Brabec, Y. Chen, L. Chen, *Angew. Chem. Int. Ed.* **2022**, 134, e202200329

[32] T. Zhang, C. An, P. Bi, Q. Lv, J. Qin, L. Hong, Y. Cui, S. Zhang, J. Hou, *Adv. Energy Mater.* **2021**, 11, 2101705.

[33] H. Feng, Y. Dai, L. Guo, D. Wang, H. Dong, Z. Liu, L. Zhang, Y. Zhu, C. Su, Y. Chen, W. Wu, *Nano Res.* **2021**, 15, 3222.